

# Heterocyclic-Additive-Activated Dinuclear Dysprosium Electrocatalysts for Heterogeneous Water Oxidation

Ching-Wei Tung,<sup>†</sup> Cheng-Han Tso,<sup>†</sup> Bo-Yi Chen, Hang Chu, Cheng-Hung Hou, Hsiao-Chien Chen, Mu-Chieh Chang, Jing-Jong Shyue, Po-Heng Lin,<sup>\*</sup> and Hao Ming Chen<sup>\*</sup>

Cite This: <https://doi.org/10.1021/acs.inorgchem.1c00209>

Read Online

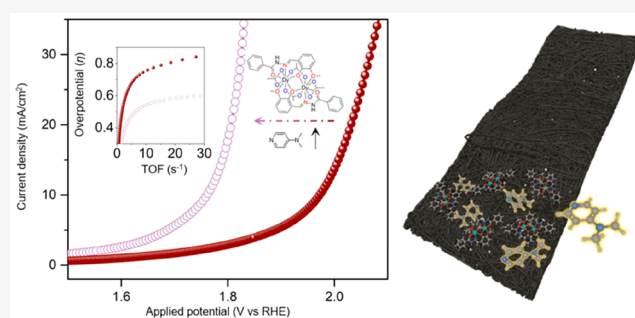
ACCESS |

Metrics & More

Article Recommendations

Supporting Information

**ABSTRACT:** Heterogeneous catalysis based on air-stable lanthanide complexes is relatively rare, especially for electrochemical water oxidation and reduction. Therefore, it is highly desired to investigate the synergy caused by cocatalysts on the lanthanide complex family for heterogeneous catalysis because of their structural diversity, air/moisture insensitivity, and easy preparation under an air atmosphere. Two mononuclear and three dinuclear dysprosium complexes containing a series of Schiff-base ligands have been demonstrated as robust electrocatalysts for triggering heterogeneous water oxidation in alkaline solution, in which the complex  $[\text{Dy}_2(\text{hmb})_2(\text{OAc})_4] \cdot \text{MeCN}(3)$  was revealed to have the best activity toward heterogeneous water oxidation among all five complexes in the present study. The molecular activation of dysprosium complexes has also been investigated with a series of N-containing heterocyclic additives [i.e., 4-(dimethylamino)pyridine (DMAP), bis(triphenylphosphine)iminium chloride ([PPN]Cl), indole, and quinoline]. In particular, the corresponding overpotential was effectively enhanced by 211 mV (at a current density of  $10 \text{ mA cm}^{-2}$ ) with the assistance of DMAP. On the basis of electrochemical and ex situ/in situ spectroscopic investigations, the best catalyst, DMAP-complex 3 on a carbon paper electrode, was confirmed with well-maintained molecular identity during heterogeneous water oxidation free of forming any dysprosium oxide and/or undesired products.



## INTRODUCTION

Inspired by natural enzymes in photosystem II, employing synthetic molecular catalysts to drive artificial photosynthesis has been investigated for decades.<sup>1–3</sup> The solar/electrical energy from renewable sources can be effectively stored via (photo)electrochemical hydrogen evolution or carbon dioxide ( $\text{CO}_2$ ) reduction, and these processes are inevitably coupled with a four-electron water oxidation ( $2\text{H}_2\text{O} \rightarrow \text{O}_2 + 4\text{H}^+ + 4\text{e}^-$ ). However, this half-reaction is regarded as a kinetic bottleneck for the above-mentioned artificial photosynthesis because it requires a significant amount of energy to trigger the multielectron-transfer processes.<sup>4,5</sup> Among the wide-range library of heterogeneous catalysts, a molecular catalyst is known for its well-defined structure, tunable design of ligand, and highly uniform active site, which can provide an opportunity to study the fundamental catalysis at the atomic level. Accordingly, numerous molecular catalysts based on noble metals, such as Ru<sup>6</sup> and Ir,<sup>7</sup> and earth-abundant transition metals, such as Mn,<sup>8</sup> Co,<sup>9</sup> Fe,<sup>10</sup> and Ni,<sup>11</sup> have been demonstrated to yield remarkably high activities toward oxygen evolution reaction (OER). Among them, multinuclear molecular complexes can offer an interesting role in this multielectron-transfer process because of their high flexibility of molecular configuration, which could afford high-valent

metal centers during OER and further suppress intramolecular ligand degradation from the multielectron transformation.<sup>12,13</sup> Numerous multinuclear complexes, such as  $[\text{Ir}(\text{pyalc})(\text{H}_2\text{O})_2(\mu\text{-O})_2]_2$ ,  $[\text{Fe}^{\text{II}}_4\text{Fe}^{\text{III}}(\mu_3\text{-O})(\mu\text{-L})_6]^{3+}$ ,  $[\text{Mn}_{12}\text{O}_{12}(\text{L})_{16}(\text{H}_2\text{O})_4]$ ,  $[(\text{bpy})\text{Cu}(\mu\text{-OH})_2(\text{OAc})_2]$ , and dimeric ruthenium catalysts, have been investigated, which allows us to bridge the concepts extracted by their mechanisms behind active intermediates and intrinsic catalytic activities in order to achieve efficient molecular catalysts.<sup>7,8,14,15</sup> A series of molecular complexes with high turnover-frequency (TOF) values for homogeneous catalysis have been revealed. However, most of them are suffering from an inadequate current and/or an unacceptable overpotential,<sup>16</sup> which plagues their practical applications at a large scale. Furthermore, metal complexes commonly require the usage of excess oxidants, specific electrolytes, and organic-solvent/water mixtures to generate active intermediates (i.e., high-valent species) in

**Special Issue:** Heterogeneous Interfaces through the Lens of Inorganic Chemistry

**Received:** January 22, 2021

homogeneous catalytic systems. The aforementioned limitations significantly circumscribe the usage of molecular complexes for triggering water splitting on an industrial scale. For this reason, incorporating molecular complexes into practical catalysis should be considered to be operated in aqueous mixtures and heterogeneous conditions.

Another strategy is to introduce molecular cocatalysts, such as pyridine base additives, that have been characteristic for enhancing the catalytic activity and product selectivity in many homogeneous catalytic systems.<sup>17,18</sup> For example, cocatalysts, such as 4-(dimethylamino)pyridine (DMAP) and bis-(triphenylphosphine)iminium chloride ([PPN]Cl), in combination with different metal complexes for promoting catalysis have been revealed.<sup>19,20</sup> The principles to improve heterogeneous catalysis have also been adopted by a polycrystalline metal electrode in electrochemical heterogeneous catalysis, which further facilitated the product formation occurring in the heterogeneous case.<sup>21,22</sup> This observation clearly confirms the fact that organic additives on film electrodes can be expected to significantly effect their catalytic activity in heterogeneous catalysis. However, the polycrystalline metal system in the literature was shown to have difficulty determining their active sites as well as actual TOF values. Furthermore, mechanistic studies on such thin-film systems are very challenging because the outermost atoms may display a behavior significantly different from that of their subsurface region (i.e., bulk region).<sup>23</sup> One possible solution to overcoming these problems is operating molecular complexes on a heterogeneous support to further clarify the correlation between the cocatalyst behavior and catalytic enhancement. On the other hand, the stability of the molecular complex is another critical issue for OER because the molecular complexes may have a high affinity for decomposing and further forming the corresponding metal oxides in aqueous solution under anodic potential.<sup>24</sup> This implies that the only solution for developing such a system is to realize a robust molecular complex in heterogeneous catalytic conditions.

Recently, the usage of rare-earth/lanthanide complexes as catalysts in both organic reactions<sup>25,26</sup> and polymerization processes<sup>27,28</sup> has attracted increasing attention. In previous work, lanthanide-based complexes containing Schiff-base ligands have been utilized for triggering CO<sub>2</sub>/epoxide copolymerization, in which all dinuclear dysprosium complexes are air-insensitive molecules and highly active in such a homogeneous catalytic system.<sup>29</sup> Indeed, heterogeneous catalysis based on air-stable lanthanide complexes is relative rare, especially for electrochemical water oxidation and reduction. Therefore, it is highly desired to investigate the synergy caused by cocatalysts on the lanthanide complex family for heterogeneous catalysis because of their structural diversity, air/moisture insensitivity, and easy preparation under an air atmosphere. Herein, two mononuclear and three dinuclear dysprosium complexes with a series of Schiff-base ligands have been used for heterogeneous oxygen evolution. Remarkably, a correlation between the organic additives and OER overpotential has been revealed, in which the [Dy<sub>2</sub>(hmb)<sub>2</sub>(OAc)<sub>4</sub>·MeCN complex can display the best performance toward heterogeneous water oxidation. We also noted that this heterogenized molecular catalyst could retain its molecular nature for long-term electrochemical catalysis, as confirmed by in situ Raman spectroscopy.

## EXPERIMENTAL SECTION

**General Materials and Methods.** All chemicals were purchased from Strem, Sigma, or Alfa Aesar without further purification. Three dinuclear complexes, [Dy<sub>2</sub>(hmb)<sub>2</sub>(OAc)<sub>4</sub>·MeCN (3·MeCN), [Dy<sub>2</sub>(hmi)<sub>2</sub>(OAc)<sub>2</sub>(MeOH)<sub>2</sub>·H<sub>2</sub>O (4·H<sub>2</sub>O), and [Dy<sub>2</sub>(hb)<sub>2</sub>(μ-OAc)<sub>2</sub>(OAc)<sub>2</sub>(H<sub>2</sub>O)<sub>2</sub>]·DMF·H<sub>2</sub>O (5·DMF·H<sub>2</sub>O), and their ligands were prepared as described in the literature.<sup>29</sup>

**Synthesis of H-hdni.** 3,5-Dinitro-2-hydroxybenzaldehyde<sup>30</sup> (20 mmol, 4.24 g) and isonicotinohydrazide (20 mmol, 2.74 g) were dissolved in 300 mL of methanol in a 500 mL round-bottom flask and refluxed for 18 h, yielding a white precipitate. The product was then filtered, washed with methanol and ether, and dried with a vacuum system to obtain 5.62 g of H-hdni (yield: 85%). <sup>1</sup>H NMR (400 MHz, DMSO-*d*<sub>6</sub>): δ 8.84 (d, 2H), 8.81 (d, 2H), 7.95 (d, 2H).

**Synthesis of H-hdmob.** 3-Methoxy-5-nitrobenzaldehyde<sup>31</sup> (20 mmol, 3.94g) and benzohydrazide (20 mmol, 2.72 g) were dissolved in 300 mL of methanol in a 500 mL round-bottom flask and refluxed for 18 h, yielding a pale-yellow precipitate. The product was then filtered, washed with methanol, and dried with a vacuum system to obtain 5.67 g of H-hdmob (yield: 90%). <sup>1</sup>H NMR (400 MHz, DMSO-*d*<sub>6</sub>): δ 8.84 (d, 2H), 8.81 (d, 2H), 7.95 (d, 2H).

**Synthesis of Complexes 1 and 2.** **Synthesis of [Dy(hmnob)(H<sub>2</sub>O)<sub>2</sub>(NO<sub>3</sub>)<sub>2</sub>]·MeCN·H<sub>2</sub>O (1·MeCN·H<sub>2</sub>O).** To a solution of Dy(NO<sub>3</sub>)<sub>3</sub>·5H<sub>2</sub>O (0.25 mmol, 0.1096 g) in methanol (15 mL) was added a solution of H-hdmob (0.25 mmol 0.0828 g) and pyridine (0.020 mL, 0.25 mmol) in methanol (15 mL). Bright-yellow crystals of the mononuclear complex 1·MeCN·H<sub>2</sub>O yielded from the resulting bright-yellow solution in 33.7% (0.0296 g) yield after 2 weeks. IR (KBr, cm<sup>-1</sup>): 3344 (br), 2266 (m), 1603 (s), 1568 (s), 1505 (w), 1484 (m), 1455 (m), 1391 (w), 1300 (s), 1260 (s), 1251 (m), 1187 (w), 1117 (m), 1097 (w), 1026 (m), 971 (m), 896 (m), 845 (m), 815 (m), 781 (w), 744 (s), 717 (s), 660 (w). Anal. Calcd for 1·MeOH·OH<sup>-</sup>: C, 29.3; H, 3.18; N, 12.06. Found: C, 29.28; H, 3.15; N, 12.05. CCDC 2056360.

**Synthesis of [Dy(hdni)<sub>2</sub>(MeOH)<sub>2</sub>]·MeOH·OH<sup>-</sup> (2·MeOH·OH<sup>-</sup>).** To a solution of Dy(NO<sub>3</sub>)<sub>3</sub>·5H<sub>2</sub>O (0.25 mmol, 0.1096 g) in methanol (15 mL) was added a solution of H-hdni (0.25 mmol 0.0828 g) and pyridine (0.020 mL, 0.25 mmol) in methanol (15 mL). The resulting yellow solution yielded yellow crystals of the mononuclear complex 2·2MeOH in 24.5% (0.0232 g) yield after 2 weeks. IR (KBr, cm<sup>-1</sup>): 3749 (s), 2988 (s), 2869 (s), 2283 (w), 1613 (m), 1560 (m), 1489 (w), 1412 (w), 1394 (m), 1305 (s), 1233 (m), 1186 (w), 1143 (w), 1102 (w), 1071 (m), 1105 (m), 925 (w), 907 (w), 840 (m), 811 (w), 787 (w), 746 (m), 717 (s), 687 (w). Anal. Calcd for 2·MeOH·OH<sup>-</sup>: C, 31.67; H, 3.65; N, 7.35. Found: C, 31.50; H, 3.65; N, 7.30. CCDC 2056361.

**Crystallographic Studies.** Single crystals of complexes 1 and 2 suitable for X-ray diffraction measurements were mounted on a Bruker D8 VENTURE diffractometer. The unit cell was determined using the Bruker SMART APEX 3 software suite to employ graphite-monochromated Mo K $\alpha$  radiation ( $\lambda = 0.71073 \text{ \AA}$ ), and the intensity data were collected with  $\omega$  scans. Data collection and reduction were performed with the CrysAlisPro software, and the absorptions were corrected by the SCALE3 ABSPACK multiscan method. The space group determination was based on the symmetry and the systematic absences displayed in the diffraction pattern. The structure was solved and refined with the Olex2 1.2-ac21 package. Anisotropic thermal parameters were used for all non-H atoms, and fixed isotropic parameters were used for H atoms.

**Electrode Fabrication.** Complexes 3–5 ( $9.296 \times 10^{-2}$  mmol each) were dispersed in 5 mL of tetrahydrofuran, and complexes 1 and 2 ( $1.859 \times 10^{-1}$  mmol each) were dispersed in 5 mL of ethanol. The mixture was treated by ultrasound for at least 30 min, and then 20  $\mu$ L of the suspension was dropped onto carbon paper (C.P.) within an area of  $0.5 \times 0.5$  cm, followed by 20  $\mu$ L of a 0.1 wt % Nafion solution after the previous layer was dried under ambient air. The 0.1 wt % Nafion solution was diluted from a commercial Nafion perfluorinated resin solution (5 wt %, Sigma) by ethanol. Finally, the mole density of the Dy ion on the electrode was  $2.975 \times 10^{-3}$  mmol cm<sup>-2</sup>. For

cocatalyst experiments,  $1.859 \times 10^{-1}$  mmol of cocatalyst was dissolved in 5 mL of tetrahydrofuran, and then 1 mL of a cocatalyst solution was mixed with 1 mL of a didysprosium suspension. The mixture was treated by ultrasound for at least 30 min, and then 40  $\mu\text{L}$  of the suspension was dropped onto C.P. within an area of  $0.5 \text{ cm} \times 0.5 \text{ cm}$ , followed by 20  $\mu\text{L}$  of a 0.1 wt % Nafion solution after the previous layer was dried under ambient air. The mole density of the Dy ion on the electrode was the same as that in the experiments without cocatalyst.

**Structural Characterization.** The morphology and elemental mapping of the specimen were performed by employing a JEM-6700F (JEOL) scanning electron microscope at 10 kV. Chemical composition analysis of the specimen was performed using a JEOL JEM-2100F field-emission scanning electron microscope equipped with an energy-dispersive spectroscopy (EDS) probe.

**Electrochemical Measurements.** All electrochemical measurements were carried out on a Bio-Logic VSP-128 potentiostat at room temperature. Pt wire and saturated calomel electrode (SCE) with a saturated KCl filling solution were used as the counter and reference electrodes, respectively. The  $\text{N}_2$ -saturated 1.0 M KOH electrolyte was prepared by bubbling  $\text{N}_2$  (99.999%) for at least 30 min. The potential versus reversible hydrogen electrode (RHE) was calculated as follows:

$$E_{\text{RHE}} = E_{\text{measure}} + E_{\text{SCE}} + 0.05916\text{pH} - iR_u \quad (1)$$

The TOF values were calculated by assuming that every Fe atom was involved in the catalysis.

$$\text{TOF} = \frac{JA}{4Fn} \quad (2)$$

The pH value of the 1 M KOH electrolyte used in this work was 14.00, and the uncompensated resistance ( $R_u$ ) was measured using potentiostatic electrochemical impedance spectroscopy (EIS). C.P. was used as the working electrode for linear-sweep voltammetry (LSV) and cyclic voltammetry (CV). Fabrication of the electrode was mentioned previously. LSV and CV were performed at a scan rate of  $100 \text{ mV s}^{-1}$ . The current densities were normalized by the working electrode geometric surface area of  $0.25 \text{ cm}^2$ .

Impedance measurements were performed for photoinduced water oxidation with a frequency range of 1.0–100 kHz. The EIS spectra were fitted by the *EC-Lab* software, and the fitting model is given in Scheme 1.

**Scheme 1. Fitting Model of the EIS Spectra**

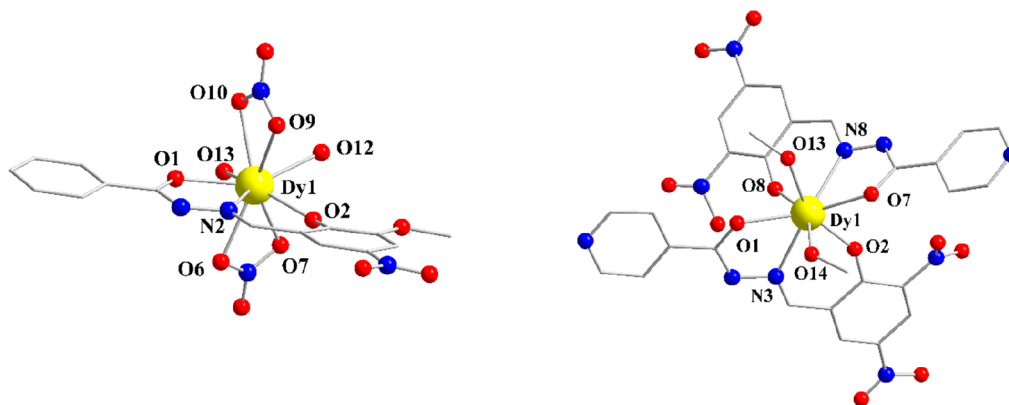
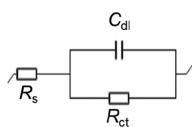


**Figure 1.** Molecular structures of complexes 1 (left) and 2 (right). Color code: Dy, yellow; O, red; N, blue; C, gray. H atoms were omitted for clarity.

**Rotating-Ring-Disk-Electrode (RRDE) Measurements.** A total of  $9.296 \times 10^{-2}$  mmol of complex 3 in 5 mL of tetrahydrofuran was dropped onto the carbon disk (area:  $0.2472 \text{ cm}^2$ ) of a RRDE tip (E7R9, Pine Research), followed by 5  $\mu\text{L}$  of a 1% Nafion solution (diluted by ethanol) after the previous layer was dried under ambient air. The speed of the RRDE was controlled by a modulated speed rotator (Pine Research) at 1600 rpm, and LSV was performed at a scan rate of  $100 \text{ mV s}^{-1}$ .

**Structural Characterization of Complex/C.P. Electrode.** The morphology of the complex/C.P. electrodes was conducted by employing a JEM-6700F (JEOL) scanning electron microscope at 15 kV. Chemical composition analysis and elemental mapping of the complex/C.P. specimen were performed using energy-dispersive X-ray analysis by a scanning electron microscope equipped with an EDS probe. X-ray photoelectron spectroscopy (XPS) analysis was done with a PHI 5000 Versa Probe (ULVAC-PHI, Japan) system, using monochromatic Al  $K\alpha$ . In order to avoid surface potential buildup during measurement, all spectra were acquired, while the sample surface was neutralized by  $e^-$  and  $\text{Ar}^+$  beams with an acceleration voltage of 10 V. In situ Raman spectra were recorded by a UniNano UNIDRON-A Raman microscopy system, employing a diode laser at 532 nm.

## RESULTS AND DISCUSSION

**Synthesis and Characterization.** The obtained 1-MeCN· $\text{H}_2\text{O}$  crystallizes in the triclinic  $P\bar{1}$  space group. A partially labeled X-ray structure of complex 1 is shown in Figure 1, and the X-ray information (including cell parameters) is given in Tables S1–S3. Selected bond distances and angles are given in Table S4. The  $\text{Dy}^{\text{III}}$  ion of the mononuclear complex adopts a nine-coordinate spherical triangular dodecahedron as determined by *SHAPE 2.1*, where one ligand, two nitrate molecules, and two coordinated  $\text{H}_2\text{O}$  molecules occupy the coordination sites. The polydentate Schiff-base ligand coordinates to the Dy center via two O atoms (O1 and O2) and one N atom (N2). Charge-balance considerations for the molecule indicate that the ligand must have one negative charge resulting from one deprotonated O2 atom and one double bond between C7 and O1. In comparison with the other reported mononuclear complex,  $[\text{Dy}(\text{hni})(\text{NO}_3)_2(\text{DMF})_2] \cdot \text{DMF}$  [ $\text{H-hni} = 2$ -hydroxyl-3-methoxy-5-nitrophenyl)methylene(isonictino)hydrazine],<sup>32</sup> it is notable that the phenyl group of  $\text{hmnob}^-$  affected the coordination environments of  $\text{Dy}^{\text{III}}$ . The two nitrate anions are on the same axis in complex 1 but vertical in the complex reported in the literature. Complex 2 crystallized in the monoclinic  $I12_1/a1$  space group (Tables S5–S7). The structure is composed of an eight-coordinated spherical

Scheme 2. Structures of Complexes 1–5 with a Series of Schiff-Base Ligands

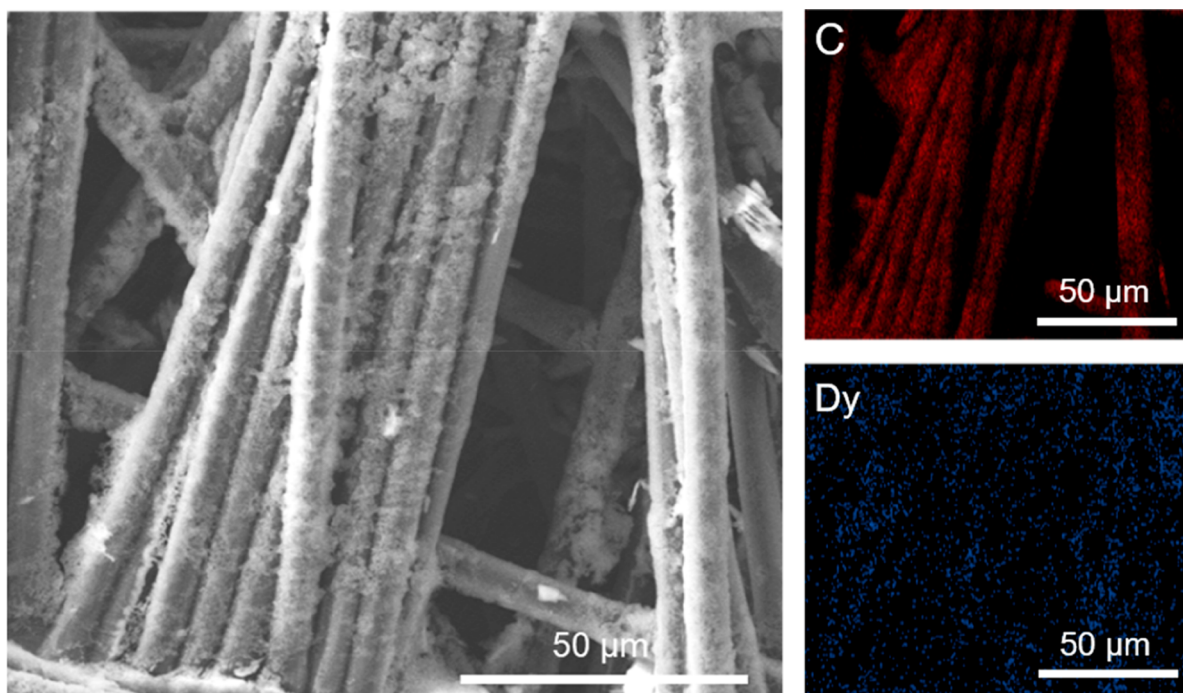
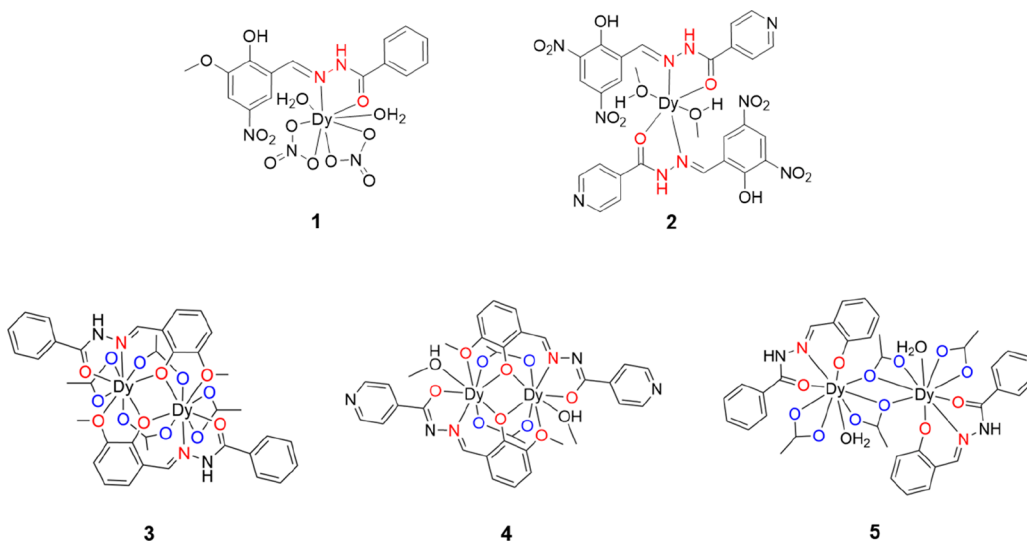
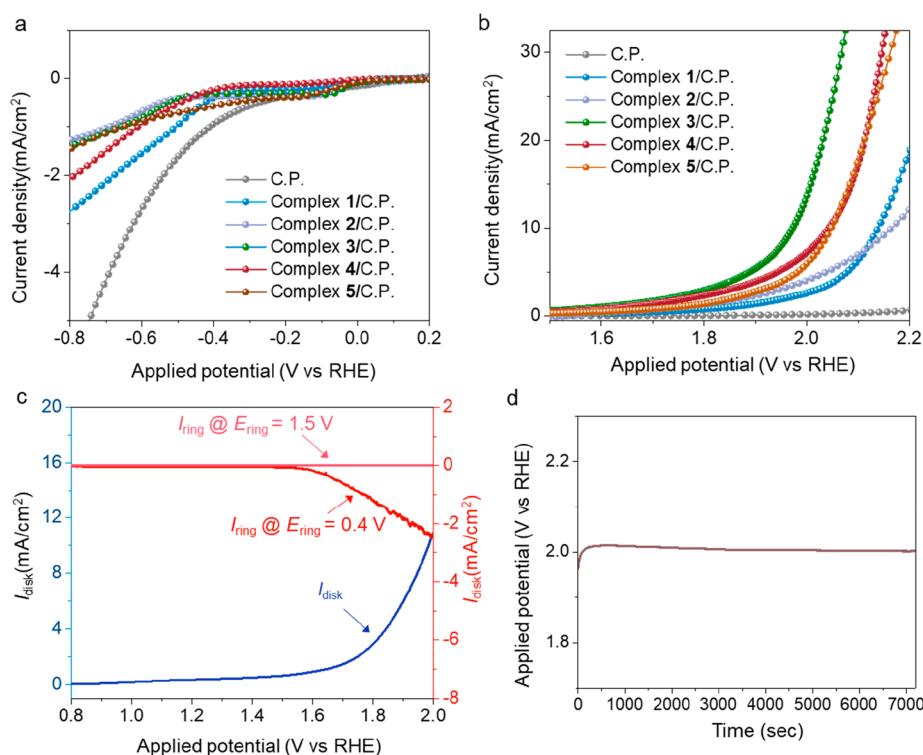


Figure 2. SEM image and corresponding elemental mapping of complex 3 on a C.P. electrode.

triangular dodecahedron  $\text{Dy}^{\text{III}}$  ion, where two ligands and two coordinated MeOH solvent molecules (O13 and O14) occupy the coordination sites. The ligands coordinated with  $\text{Dy}^{\text{III}}$  in the same coordination modes as complex 1 as the keto form of  $\text{hmnob}^-$ . The figures of packing arrangements and the asymmetric units for complexes 1 and 2 are also shown in Figures S1 and S2. Furthermore, because of the necessity for charge balance, the  $\text{OH}^-$  ion was also present within the lattice structure. Three dinuclear dysprosium complexes, 3–5, were also synthesized for further catalytic studies (Scheme 2) in order to compare the catalytic activities between mono- and dinuclear systems. The scanning electron microscopy (SEM) image and corresponding elemental mapping of complex 3 on a C.P. electrode are shown in Figure 2 (left) as an example, which revealed that the molecular catalyst was well-distributed, loading onto the carbon support because of the presence of the

surface texture. Elemental mapping with EDS, as illustrated in Figure 2 (right), verified the obvious presence of dysprosium on the C.P. electrode.

**Heterogeneous Water Oxidation Performance.** The electrochemical behaviors of a series of dysprosium complexes on C.P. electrodes for both water reduction and oxidation were investigated with LSV in a 1.0 M KOH solution. As shown in Figure 3a, the presence of a reductive current from  $\sim 0.1$  to  $\sim -0.4$  V (vs RHE) was related to the reduction of  $\text{Dy}^{\text{III}}$  in two steps ( $\text{Dy}^{\text{III}} + \text{e}^- \rightarrow \text{Dy}^{\text{II}}$  and  $\text{Dy}^{\text{II}} + 2\text{e}^- \rightarrow \text{Dy}^0$ ). This phenomenon indicated that these dysprosium complexes are unable to maintain their metal sites in the ligand-coordinated environment under cathodic potential in an alkaline electrolyte. Besides, as for the cathodic scan, the activities of all catalysts under identical conditions revealed that the loading of dysprosium complexes would have a smaller current response



**Figure 3.** Electrochemical water oxidation properties of dysprosium molecular complexes onto C.P. (a) HER and (b) OER polarization curves of complexes 1–5/C.P. in 1.0 M KOH at a scan rate of 20 mV s<sup>-1</sup> with *iR* compensation. (c) RRDE measurement of a 3 catalyst in O<sub>2</sub>-saturated 1.0 M KOH (rotation speed of 1600 rpm). (d) Potential versus time data on complex 3/C.P. in 1.0 M KOH for 2 h at a constant current density of 10 mA cm<sup>-2</sup> (vs RHE), in which no significant decay was observed.

and a larger onset potential than those of a bare C.P. electrode. This phenomenon suggests that the formation of dysprosium(0) species from heterogeneous conditions has no significant activity for triggering hydrogen evolution reaction (HER; i.e., water reduction). In contrast, as for the anodic scan, we were able to clarify the remarkably electrocatalytic OER activity for complexes 1–5 on C.P. compared to that of a bare C.P. electrode. Among all complexes, complex 3/C.P. was revealed to exhibit the lowest overpotential ( $\eta$ ) at a current density of 10 mA cm<sup>-2</sup> (the current response necessary for about 10% efficient solar-to-fuel conversion)<sup>33</sup> compared to those of the mononuclear complexes of 1/C.P. and 2/C.P. Furthermore, the other two dinuclear dysprosium complexes, 4/C.P. and 5/C.P., were observed to have better activities than those of mononuclear complexes, which indicated an interesting interplay as a consequence of adjacent dysprosium (*vide infra*). Accordingly, significant cathodic shifts of 813 and 817 mV can be achieved in the overpotential compared with complexes 1/C.P. ( $\eta = 908$  mV) and 2/C.P. ( $\eta = 935$  mV), respectively, because of the contribution from the adjacent dysprosium.

The combination of molecular complexes and a heterogeneous catalytic system could maximize atomic utilization; moreover, the amount of metallic waste from electrode fabrication and catalytic reaction could be suppressed. That is, the loading amount of complex 3/C.P. was also optimized to achieve an optimal condition with atomic-scale precision ( $\sim 3.0$   $\mu\text{mol cm}^{-2}$ ; Figure S3). The Tafel slopes for dinuclear complexes (259 mV dec<sup>-1</sup> for complex 3, 282 mV dec<sup>-1</sup> for complex 4, and 301 mV dec<sup>-1</sup> for complex 5) are much smaller than those of mononuclear complexes (363 mV dec<sup>-1</sup> for complex 1 and 354 mV dec<sup>-1</sup> for complex 2), suggesting that

superior kinetics of water oxidation could have arisen from complexes with a dinuclear oxygen-bridged nature (Figure S4). Besides, the SEM images confirm that the lower activity of complexes 1 and 2 is not due to the distribution of catalysts on carbon supports (Figure S5). To further confirm the production of oxygen gas, a RRDE investigation was carried out, as shown in Figure 3c. A cathodic current was detected on the ring electrode at +0.4 V, together with a rise of the OER current on the disk electrode, demonstrating that once the oxygen gas was formed on the disk electrode, oxygen reduction took place on the ring electrode. Moreover, a negligible current density on the ring electrode (at +1.5 V) suggested that OER occurred through a four-electron pathway ( $4\text{OH}^- \rightarrow \text{O}_2 + 2\text{H}_2\text{O} + 4\text{e}^-$ ). The above RRDE analysis clarified that the bubbles generated from complex 3/C.P. were exactly oxygen gas, and the main current response was attributed to electrochemical water oxidation. The robust stability was also validated in a chronopotentiometry measurement, where only a slight decay in the applied potential for achieving 10 mA cm<sup>-2</sup> was observed after working for 2 h (Figure 3d). This manifests that the complex of 3/C.P. can act as a practical and robust electrocatalyst for heterogeneous oxygen evolution. Consequently, the chemical robustness of the present dysprosium molecular electrocatalyst in an alkaline environment could be appropriately utilized to further reveal the synergic effects of cocatalysts toward OER electrocatalysis.

**Molecular-Cocatalyst-Assisted Water Oxidation.** Inspired by the previously reported OER activity as a result of different metal–N coordination environments of single-atom electrocatalysts, we postulated that the character of N-containing heterocyclic additives may affect the OER behaviors of molecular complexes under heterogeneous catalytic

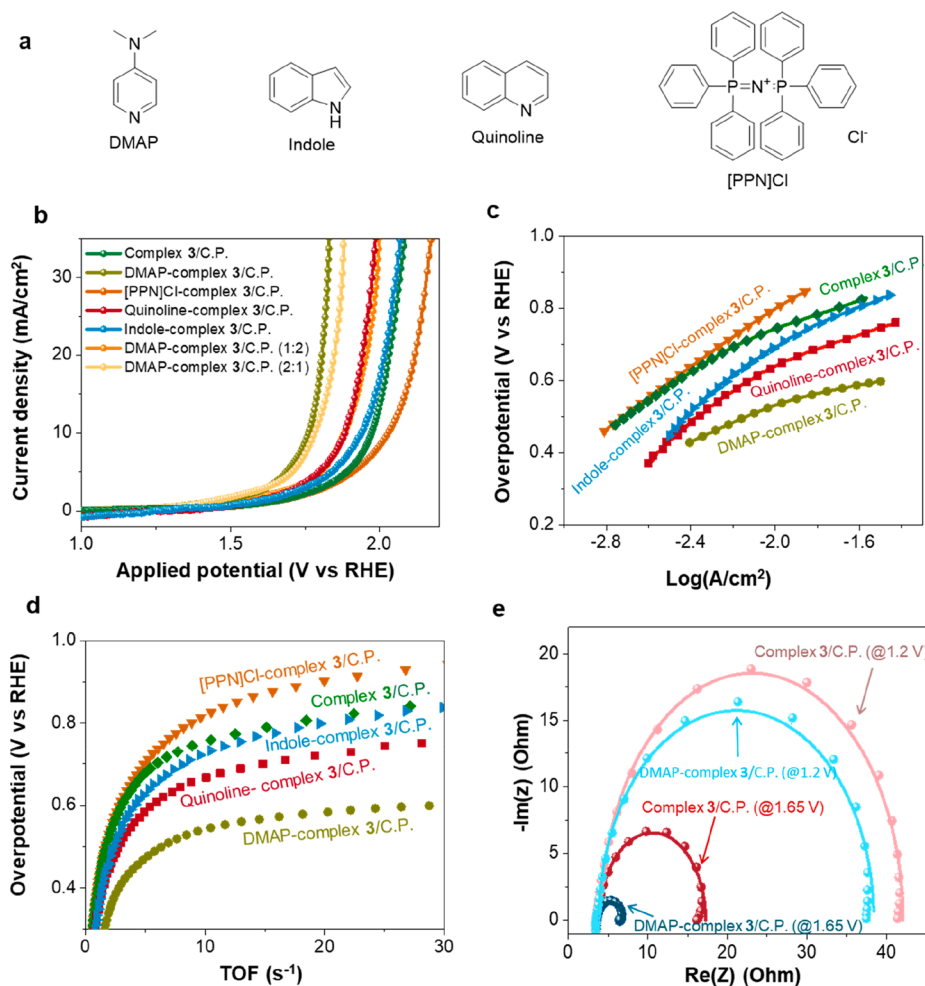


**Figure 4.** (a) Molecular structures of N-containing heterocyclic additives, including DMAP, indole, quinoline, and [PPN]Cl. (b) OER polarization curves and (c) Tafel slopes (overpotential vs log current) of complex 3/C.P. in 1.0 M KOH with different cocatalysts. (d) TOF values versus overpotential of complex 3/C.P. and cocatalyst–complex 3/C.P. (e) Nyquist plots of complex 3/C.P. and cocatalyst–complex 3/C.P. measured in 1.0 M KOH at applied potentials of 1.2 and 1.65 V.

conditions.<sup>34</sup> A series of N-containing heterocyclic additives (DMAP, indole, quinoline, and [PPN]Cl) were introduced to alter OER electrocatalysis of complex 3/C.P. as the cocatalyst (Figure 4a), in which the as-prepared electrodes consist of a mixture of dysprosium complexes, Nafion membranes, and heterocyclic additive cocatalysts. The corresponding OER catalytic nature of these functionalized electrodes was clarified by LSV in a 1.0 M KOH solution (Figure 4b). Impressively, the presence of N-containing heterocyclic additives showed an evident difference on their overpotential from that of the original complex 3/C.P. Except for the addition of [PPN]Cl, the incorporation of pyridine- and indole-based cocatalysts into complex 3/C.P. demonstrated remarkably enhanced activity toward water oxidation. The addition of DMAP resulted in the best performance ( $\eta = 531$  mV) among this series, which could shift the overpotential cathodically at a current density of  $10 \text{ mA cm}^{-2}$  by 211 mV compared with complex 3/C.P. ( $\eta = 742$  mV). Comparing the activity among all catalysts under identical conditions indicated that quinoline–complex 3/C.P. ( $\eta = 653$  mV) and indole–complex 3/C.P. ( $\eta = 710$  mV) were poorly active, which indicated that the different  $\sigma$ -donating characters of heterocyclic additives could significantly affect the local environment (i.e., isostructurality) around the catalytic center.<sup>35,36</sup> Among these functionalized

electrodes, only [PPN]Cl–complex 3/C.P. presented a clear decline in the resulting activity, which may be due to the bulky cations of PPN that can suppress the formation of reaction intermediates from the  $\text{Dy}^{\text{III}}$  metal center for OER. Notably, the functionalized electrode formed in the presence of pyridine-based additives exhibited a significant enhancement in the overpotential, especially for the case of DMAP activation. Accordingly, the influence of the N atom around metal centers toward OER was confirmed by preparing the electrodes with various ratios of Dy/DMAP (1:1, 1:2, and 2:1). As shown in Figure 4b, the overpotential changed slightly with an increasing amount of DMAP but dramatically increased with a 2:1 ratio of the Dy site and DMAP. The dependence of the DMAP ratio indicates that the addition of a cocatalyst plays a central role in these heterogenized molecular catalysts. The Tafel slopes were calculated to understand the electrocatalytic OER kinetics, as shown in Figure 4c. In line with the polarization curves, DMAP–complex 3/C.P. endows the smallest Tafel slope ( $164 \text{ mV dec}^{-1}$ ), much lower than those of quinoline–complex 3/C.P. ( $209 \text{ mV dec}^{-1}$ ), indole–complex 3/C.P. ( $235 \text{ mV dec}^{-1}$ ), and [PPN]Cl–complex 3/C.P. ( $323 \text{ mV dec}^{-1}$ ). These results manifested that the OER kinetics of complex 3/C.P. was essentially improved by introducing N-containing heterocyclic additives. To mechanis-

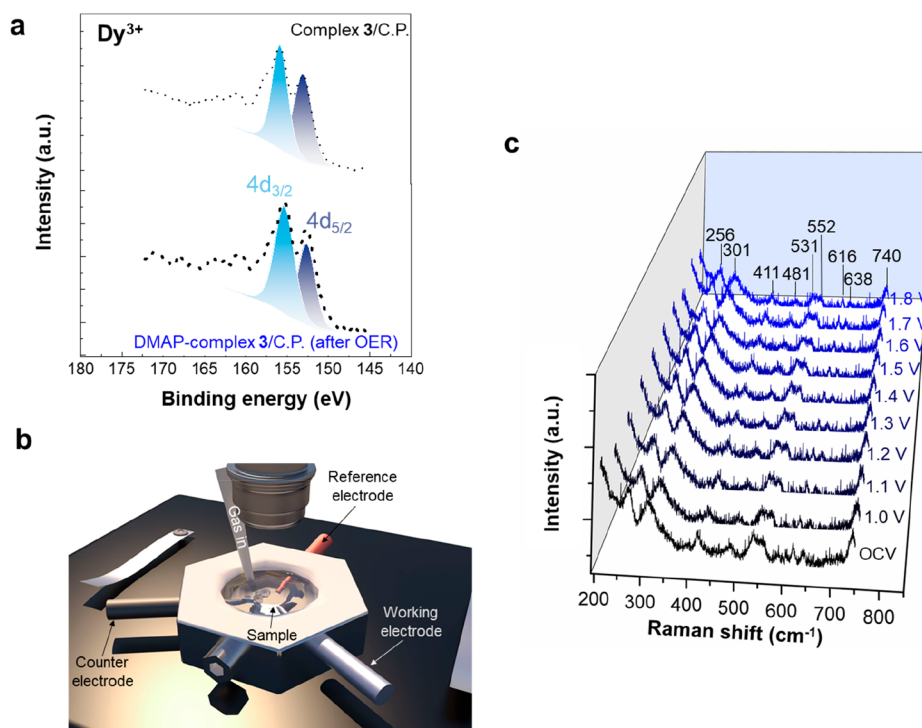


**Figure 5.** (a) XPS spectra of complex 3/C.P. (top) and DMAP–complex 3/C.P. taken after 2 h of heterogeneous water oxidation (bottom) at a current density of  $10 \text{ mA cm}^{-2}$ . (b) Schematic diagram of an in situ Raman apparatus applied to a customized liquid cell. (c) Raman spectra of DMAP–complex 3/C.P. versus control potentials in 1.0 M KOH.

tically investigate the interplay between the cocatalyst and complex 3/C.P., the TOF of the dysprosium complex was estimated to evaluate the intrinsic activity of the series of cocatalyst–complex 3/C.P., which referred to the activity per metal site in a heterogeneous reaction (Figure 4d). DMAP–complex 3/C.P. could exhibit excellent electrocatalytic activity; for example, the overpotential required to achieve a TOF of  $10 \text{ s}^{-1}$  was only 541 mV, which was much lower than those of quinoline–complex 3/C.P. (667 mV), indole–complex 3/C.P. (726 mV), [PPN]Cl–complex 3/C.P. (820 mV), and complex 3/C.P. (755 mV). The TOF value of DMAP–complex 3/C.P. and corresponding overpotential were presented along with the values of some molecular catalysts for heterogeneous catalysis, such as dinuclear iridium complexes (with 100 equiv of  $\text{NaIO}_4$ ) and mononuclear transition-metal complexes, as shown in Table S8. This clearly shows that the TOF value of DMAP–complex 3/C.P. is comparable with that of  $[\text{Ir}(\text{pyalc})(\text{H}_2\text{O})_2(\mu\text{-O})]_2$  (TOF =  $7.9 \text{ s}^{-1}$  at  $\eta = 520 \text{ mV}$ )<sup>7</sup> and relatively high compared to that of  $\text{Fe}(\text{TAMLS})\text{H}_2\text{O}$  (TOF =  $0.081 \text{ s}^{-1}$  at  $\eta = 750 \text{ mV}$ ).<sup>37</sup> Additionally, prolonged testing of DMAP–complex 3/C.P. at a constant current density of  $10 \text{ mA cm}^{-2}$  was performed to reveal a steady applied potential for 2 h without noticeable decay (Figure S6). SEM images also confirmed the robustness of DMAP–complex 3 on carbon supports after OER in heterogeneous conditions (Figure S7). Furthermore, impedance measurement was performed to investigate the interfacial properties of electrodes at various voltages near the OER region. The semicircular regions in the Nyquist impedance plots and these curves were fitted by using a proposed equivalent circuit (Table S9), which included the charge-transfer resistance ( $R_{\text{ct}}$ ), double-layer capacitance ( $C_{\text{dl}}$ ), and solution resistance ( $R_s$ ). As shown in Figure 4e, the addition of DMAP to complex 3/C.P. was unable to substantially alter the feature of the semicircular

region before OER onset (+1.2 V). Once a potential beyond the OER onset was applied,  $R_{\text{ct}}$  of DMAP–complex 3/C.P. ( $3.5 \Omega$ ) decreased significantly to  $12.6 \Omega$ . This observation indicated that the addition of DMAP can effectively enhance the charge-transfer processes at the catalyst/electrolyte interface during OER. In addition, the increase in  $C_{\text{dl}}$  of DMAP–complex 3/C.P. at +1.65 V ( $1.4 \text{ mF cm}^{-2}$ ) reflected its effective electrochemical active surface area. The above results revealed that the remarkable enhancement in OER kinetics can be attributed to the incorporation of N-containing heterocyclic additives into the heterogenized molecular electrode. Moreover, we validated the evidence that the ratio between organic additives and active sites could be accurately manipulated in heterogeneous electrochemical systems, which allowed us to design a more efficient electrocatalytic system. Operating molecular complexes on heterogeneous supports offered available information to further understand how to enhance the activity with the assistance of cocatalysts in practical electrochemical conditions. This system evidently is able to combine the organic molecules and metal complexes that contain well-defined active sites at the atomic scale for triggering heterogeneous catalysis.

It is paramount to clarify that the ligand-coordinated complexes are robust and able to remain steady during OER in heterogeneous conditions. According to the XPS spectra (Figures 5a and S8 and S9), it is shown that complex 3 was able to robustly maintain the original molecular structure on the C.P. electrode ( $153$  and  $156 \text{ cm}^{-1}$  for  $4d_{5/2}$  and  $4d_{3/2}$ , respectively), indicating that the metal centers are still coordinated by a Schiff-base ligand after heterogeneous electrocatalysis at a current density of  $10 \text{ mA cm}^{-2}$  for 2 h. To further realize the robustness of complex 3 for acting as a molecular catalyst during electrocatalysis, in situ Raman spectra of DMAP–complex 3/C.P. were performed as

illustrated in Figure 5b.<sup>38,39</sup> Indeed, the results revealed that the peaks of complex 3 were evidently observed and steady at applied anodic potentials, while no other features (374, 464, and 585 cm<sup>-1</sup>) as a result of metal oxide formation<sup>40</sup> were shown in electrochemical oxidation (Figures 5c and S10). Consequently, we can conclude that its molecular identity was maintained during heterogeneous water oxidation without forming any dysprosium oxide and/or undesired products.

## CONCLUSION

In summary, a simple and tunable system in atomic scale for heterogeneous water oxidation with the synergy of an additional molecular cocatalyst has been realized. A series of N-containing heterocyclic additives were successfully employed to enhance the OER activity of the dysprosium complex. Even though the OER overpotentials of our rare-earth complexes are relatively higher than those of other noble- or transition-metal catalysts, it still offers the possibility of studying fundamental aspects of heterogeneous catalytic reaction, especially for how the different  $\sigma$ -donating characters of organic additives influence the activity of heterogenized molecular complexes. In particular, selecting DMAP as a cocatalyst was revealed to significantly improve the onset potential of complex 3/C.P. for triggering the water oxidation reaction. The molecular complex was robust after periods of OER testing in heterogeneous conditions, as confirmed by XPS and in situ Raman spectroscopy. These results not only provided the first demonstration of applying rare-earth molecular complexes for OER, the strategy of the combination of N-containing heterocyclic additives, and a heterogenized molecular electrode but also established a prototype for scalably tuning the OER catalyst at the atomic scale and offered fundamental knowledge for future investigations of OER in heterogeneous conditions.

## ASSOCIATED CONTENT

### Supporting Information

The Supporting Information is available free of charge at <https://pubs.acs.org/doi/10.1021/acs.inorgchem.1c00209>.

Packing arrangements, polarization curves, Tafel slopes, SEM images and corresponding elemental mapping, potential versus time data, and XPS and Raman spectra (Figures S1–S10) and crystallographic data, selected angles and bond lengths, calculation results, comparison of TOF values, and  $R_s$ ,  $R_{ct}$ , and  $C_{dl}$  values fit from the EIS data, and (Tables S1–S9) (PDF)

### Accession Codes

CCDC 2056360 and 2056361 contain the supplementary crystallographic data for this paper. These data can be obtained free of charge via [www.ccdc.cam.ac.uk/data\\_request/cif](http://www.ccdc.cam.ac.uk/data_request/cif), or by emailing [data\\_request@ccdc.cam.ac.uk](mailto:data_request@ccdc.cam.ac.uk), or by contacting The Cambridge Crystallographic Data Centre, 12 Union Road, Cambridge CB2 1EZ, UK; fax: +44 1223 336033.

## AUTHOR INFORMATION

### Corresponding Authors

Po-Heng Lin – Department of Chemistry, National Chung Hsing University, Taichung 402, Taiwan; [orcid.org/0000-0002-0893-0806](https://orcid.org/0000-0002-0893-0806); Email: [poheng@dragon.nchu.edu.tw](mailto:poheng@dragon.nchu.edu.tw)

Hao Ming Chen – Department of Chemistry, National Taiwan University, Taipei 106, Taiwan; [orcid.org/0000-0002-7480-9940](https://orcid.org/0000-0002-7480-9940); Email: [haomingchen@ntu.edu.tw](mailto:haomingchen@ntu.edu.tw)

### Authors

Ching-Wei Tung – Department of Chemistry, National Taiwan University, Taipei 106, Taiwan

Cheng-Han Tso – Department of Chemistry, National Taiwan University, Taipei 106, Taiwan

Bo-Yi Chen – Department of Chemistry, National Chung Hsing University, Taichung 402, Taiwan

Hang Chu – Department of Chemistry, National Taiwan University, Taipei 106, Taiwan

Cheng-Hung Hou – Research Center for Applied Sciences, Academia Sinica, Taipei 106, Taiwan; [orcid.org/0000-0002-5150-7106](https://orcid.org/0000-0002-5150-7106)

Hsiao-Chien Chen – Center for Reliability Science and Technologies, Chang Gung University, Taoyuan 333, Taiwan

Mu-Chieh Chang – Department of Chemistry, National Taiwan University, Taipei 106, Taiwan; [orcid.org/0000-0002-7270-0319](https://orcid.org/0000-0002-7270-0319)

Jing-Jong Shyue – Research Center for Applied Sciences, Academia Sinica, Taipei 106, Taiwan; [orcid.org/0000-0002-8508-659X](https://orcid.org/0000-0002-8508-659X)

Complete contact information is available at: <https://pubs.acs.org/doi/10.1021/acs.inorgchem.1c00209>

### Author Contributions

<sup>†</sup>The manuscript was written through contributions of all authors. All authors have given approval to the final version of the manuscript. These authors contributed equally to this work.

### Notes

The authors declare no competing financial interest.

## ACKNOWLEDGMENTS

We acknowledge support from the Ministry of Science and Technology, Taiwan (Contracts MOST 108-2628-M-002-004-RSP and MOST 109-2113-M-005-019).

## REFERENCES

- (1) Bard, A. J.; Fox, M. A. Artificial Photosynthesis: Solar Splitting of Water to Hydrogen and Oxygen. *Acc. Chem. Res.* **1995**, *28* (3), 141–145.
- (2) Garrido-Barros, P.; Gimbert-Suriñach, C.; Matheu, R.; Sala, X.; Llobet, A. How to make an efficient and robust molecular catalyst for water oxidation. *Chem. Soc. Rev.* **2017**, *46* (20), 6088–6098.
- (3) Zhang, B.; Sun, L. Artificial photosynthesis: opportunities and challenges of molecular catalysts. *Chem. Soc. Rev.* **2019**, *48* (7), 2216–2264.
- (4) Suen, N.-T.; Hung, S.-F.; Quan, Q.; Zhang, N.; Xu, Y.-J.; Chen, H. M. Electrocatalysis for the oxygen evolution reaction: recent development and future perspectives. *Chem. Soc. Rev.* **2017**, *46* (2), 337–365.
- (5) Tung, C.-W.; Hsu, Y.-Y.; Shen, Y.-P.; Zheng, Y.; Chan, T.-S.; Sheu, H.-S.; Cheng, Y.-C.; Chen, H. M. Reversible adapting layer produces robust single-crystal electrocatalyst for oxygen evolution. *Nat. Commun.* **2015**, *6*, 8106.
- (6) Matheu, R.; Ertem, M. Z.; Benet-Buchholz, J.; Coronado, E.; Batista, V. S.; Sala, X.; Llobet, A. Intramolecular Proton Transfer Boosts Water Oxidation Catalyzed by a Ru Complex. *J. Am. Chem. Soc.* **2015**, *137* (33), 10786–10795.
- (7) Sheehan, S. W.; Thomsen, J. M.; Hintermair, U.; Crabtree, R. H.; Brudvig, G. W.; Schmittenmaier, C. A. A molecular catalyst for

water oxidation that binds to metal oxide surfaces. *Nat. Commun.* **2015**, *6* (1), 6469.

(8) Maayan, G.; Gluz, N.; Christou, G. A bioinspired soluble manganese cluster as a water oxidation electrocatalyst with low overpotential. *Nat. Catal.* **2018**, *1* (1), 48–54.

(9) Huang, B.; Wang, Y.; Zhan, S.; Ye, J. One-step electrochemical deposition of Schiff base cobalt complex as effective water oxidation catalyst. *Appl. Surf. Sci.* **2017**, *396*, 121–128.

(10) Fillol, J. L.; Codolà, Z.; Garcia-Bosch, I.; Gómez, L.; Pla, J. J.; Costas, M. Efficient water oxidation catalysts based on readily available iron coordination complexes. *Nat. Chem.* **2011**, *3* (10), 807–813.

(11) Masud, J.; Ioannou, P.-C.; Levesanos, N.; Kyritsis, P.; Nath, M. A Molecular Ni-complex Containing Tetrahedral Nickel Selenide Core as Highly Efficient Electrocatalyst for Water Oxidation. *ChemSusChem* **2016**, *9* (22), 3128–3132.

(12) Duan, L.; Bozoglian, F.; Mandal, S.; Stewart, B.; Privalov, T.; Llobet, A.; Sun, L. A molecular ruthenium catalyst with water-oxidation activity comparable to that of photosystem II. *Nat. Chem.* **2012**, *4* (5), 418–423.

(13) Cox, N.; Pantazis, D. A.; Neese, F.; Lubitz, W. Biological Water Oxidation. *Acc. Chem. Res.* **2013**, *46* (7), 1588–1596.

(14) Su, X.-J.; Gao, M.; Jiao, L.; Liao, R.-Z.; Siegbahn, P. E. M.; Cheng, J.-P.; Zhang, M.-T. Electrocatalytic Water Oxidation by a Dinuclear Copper Complex in a Neutral Aqueous Solution. *Angew. Chem., Int. Ed.* **2015**, *54* (16), 4909–4914.

(15) Okamura, M.; Kondo, M.; Kuga, R.; Kurashige, Y.; Yanai, T.; Hayami, S.; Praneeth, V. K. K.; Yoshida, M.; Yoneda, K.; Kawata, S.; Masaoka, S. A pentanuclear iron catalyst designed for water oxidation. *Nature* **2016**, *530* (7591), 465–468.

(16) Lloret-Fillol, J.; Costas, M. Water oxidation: High five iron. *Nat. Energy* **2016**, *1* (3), 16023.

(17) Barton Cole, E.; Lakkaraju, P. S.; Rampulla, D. M.; Morris, A. J.; Abelev, E.; Bocarsly, A. B. Using a One-Electron Shuttle for the Multielectron Reduction of CO<sub>2</sub> to Methanol: Kinetic, Mechanistic, and Structural Insights. *J. Am. Chem. Soc.* **2010**, *132* (33), 11539–11551.

(18) Rosen, B. A.; Salehi-Khojin, A.; Thorson, M. R.; Zhu, W.; Whipple, D. T.; Kenis, P. J. A.; Masel, R. I. Ionic Liquid-Mediated Selective Conversion of CO<sub>2</sub> to CO at Low Overpotentials. *Science* **2011**, *334* (6056), 643.

(19) Darensbourg, D. J.; Mackiewicz, R. M. Role of the Cocatalyst in the Copolymerization of CO<sub>2</sub> and Cyclohexene Oxide Utilizing Chromium Salen Complexes. *J. Am. Chem. Soc.* **2005**, *127* (40), 14026–14038.

(20) Darensbourg, D. J.; Mackiewicz, R. M.; Rodgers, J. L.; Phelps, A. L. (Salen)Cr(III) Catalysts for the Copolymerization of Carbon Dioxide and Epoxides: Role of the Initiator and Cocatalyst. *Inorg. Chem.* **2004**, *43* (6), 1831–1833.

(21) Han, Z.; Kortlever, R.; Chen, H.-Y.; Peters, J. C.; Agapie, T. CO<sub>2</sub> Reduction Selective for C ≥ 2 Products on Polycrystalline Copper with N-Substituted Pyridinium Additives. *ACS Cent. Sci.* **2017**, *3* (8), 853–859.

(22) Hahn, C.; Jaramillo, T. F. Using Microenvironments to Control Reactivity in CO<sub>2</sub> Electrocatalysis. *Joule* **2020**, *4* (2), 292–294.

(23) Roy, C.; Sebok, B.; Scott, S. B.; Fiordaliso, E. M.; Sørensen, J. E.; Bodin, A.; Trimarco, D. B.; Damsgaard, C. D.; Vesborg, P. C. K.; Hansen, O.; Stephens, I. E. L.; Kibsgaard, J.; Chorkendorff, I. Impact of nanoparticle size and lattice oxygen on water oxidation on NiFeOxHy. *Nat. Catalysis* **2018**, *1* (11), 820–829.

(24) Wu, X.; Li, F.; Zhang, B.; Sun, L. Molecular complexes in water oxidation: Pre-catalysts or real catalysts. *J. Photochem. Photobiol., C* **2015**, *25*, 71–89.

(25) Chiu, T.-Y.; Chin, W.; Guo, J.-R.; Liang, C.-F.; Lin, P.-H. A Dinuclear Dysprosium Complex as an Air-Stable and Recyclable Catalyst: Applications in the Deacetylation of Carbohydrate, Aliphatic, and Aromatic Molecules. *Chem.—Asian J.* **2019**, *14* (5), 627–633.

(26) Lu, C.; Hu, L.; Zhao, B.; Yao, Y. Addition of Thiols to Isocyanates Catalyzed by Simple Rare-Earth-Metal Amides: Synthesis of S-Alkyl Thiocarbamates and Dithiocarbamates. *Organometallics* **2019**, *38* (9), 2167–2173.

(27) Su, Y.-C.; Chiu, T.-Y.; Liu, Y.-T.; Lin, P.-H.; Ko, B.-T. Significant enhancement of catalytic properties in mononuclear yttrium complexes by nitrophenolate-type ligands: Synthesis, structure, and catalysis for lactide polymerization. *J. Polym. Sci., Part A: Polym. Chem.* **2019**, *57* (19), 2038–2047.

(28) Peewasan, K.; Merkel, M. P.; Fuhr, O.; Powell, A. K. A designed and potentially decadenate ligand for use in lanthanide(III) catalyzed biomass transformations: targeting diastereoselective trans-4,5-diaminocyclopentenone derivatives. *Dalton Trans.* **2020**, *49* (7), 2331–2336.

(29) Ho, C.-H.; Chuang, H.-J.; Lin, P.-H.; Ko, B.-T. Copolymerization of carbon dioxide with cyclohexene oxide catalyzed by bimetallic dysprosium complexes containing hydrazine-functionalized Schiff-base derivatives. *J. Polym. Sci., Part A: Polym. Chem.* **2017**, *55* (2), 321–328.

(30) Abdullah, A.; Nevell, T. G.; Sammes, P. G.; Roxburgh, C. J. Unusual thermo(photo)chromic properties of some mononitro- and dinitro- substituted 3'-alkyl indolospirobenzopyrans. *Dyes Pigm.* **2015**, *121*, 57–72.

(31) Darwish, N.; Aragonès, A. C.; Darwish, T.; Ciampi, S.; Díez-Pérez, I. Multi-Responsive Photo- and Chemo-Electrical Single-Molecule Switches. *Nano Lett.* **2014**, *14* (12), 7064–7070.

(32) Cheng, L.-W.; Zhang, C.-L.; Wei, J.-Y.; Lin, P.-H. Mononuclear and trinuclear Dy(III) SMMs with Schiff-base ligands modified by nitro-groups: first triangular complex with a N-N pathway. *Dalton Trans.* **2019**, *48* (46), 17331–17339.

(33) Walter, M. G.; Warren, E. L.; McKone, J. R.; Boettcher, S. W.; Mi, Q.; Santori, E. A.; Lewis, N. S. Solar Water Splitting Cells. *Chem. Rev.* **2010**, *110* (11), 6446–6473.

(34) Xu, H.; Cheng, D.; Cao, D.; Zeng, X. C. A universal principle for a rational design of single-atom electrocatalysts. *Nat. Catal.* **2018**, *1* (5), 339–348.

(35) Meihaus, K. R.; Minasian, S. G.; Lukens, W. W.; Kozimor, S. A.; Shuh, D. K.; Tylliszczak, T.; Long, J. R. Influence of Pyrazolate vs N-Heterocyclic Carbene Ligands on the Slow Magnetic Relaxation of Homoleptic Trischelate Lanthanide(III) and Uranium(III) Complexes. *J. Am. Chem. Soc.* **2014**, *136* (16), 6056–6068.

(36) Wu, H.; Wu, Q.-Y.; Wang, C.-Z.; Lan, J.-H.; Liu, Z.-R.; Chai, Z.-F.; Shi, W.-Q. New insights into the selectivity of four 1,10-phenanthroline-derived ligands toward the separation of trivalent actinides and lanthanides: a DFT based comparison study. *Dalton Transactions* **2016**, *45* (19), 8107–8117.

(37) Coggins, M. K.; Zhang, M.-T.; Vannucci, A. K.; Dares, C. J.; Meyer, T. J. Electrocatalytic Water Oxidation by a Monomeric Amidate-Ligated Fe(III)-Aqua Complex. *J. Am. Chem. Soc.* **2014**, *136* (15), 5531–5534.

(38) Zhu, Y.; Wang, J.; Chu, H.; Chu, Y.-C.; Chen, H. M. In Situ/Operando Studies for Designing Next-Generation Electrocatalysts. *ACS Energy Lett.* **2020**, *5* (4), 1281–1291.

(39) Chang, C.-J.; Zhu, Y.; Wang, J.; Chen, H.-C.; Tung, C.-W.; Chu, Y.-C.; Chen, H. M. In situ X-ray diffraction and X-ray absorption spectroscopy of electrocatalysts for energy conversion reactions. *J. Mater. Chem. A* **2020**, *8* (37), 19079–19112.

(40) Sharma, N. D.; Singh, J.; Dogra, S.; Varandani, D.; Poswal, H. K.; Sharma, S. M.; Bandyopadhyay, A. K. Pressure-induced anomalous phase transformation in nano-crystalline dysprosium sesquioxide. *J. Raman Spectrosc.* **2011**, *42* (3), 438–444.